Polyelectrolytes in Electric Fields†

R. R. Netz

Sektion Physik, LMU Munich, Theresienstrasse 37, 80333 Munich, Germany

Received: December 18, 2002; In Final Form: May 7, 2003

We investigate the effect of an electric field on a highly charged polyelectrolyte (PE) chain by Brownian-dynamics simulation methods and a combination of different scaling arguments. In the simulation we take the counterions explicitly into account and therefore include the effects of counterion condensation and PE collapse as the coupling parameter (proportional to counterion valency) is increased. For highly charged PEs in the collapsed phase, a nonequilibrium unfolding transition occurs at sufficiently high electric fields where the PE aligns parallel to the external field. The critical field strength E^* is determined from scaling results for the polarizability of a PE globule and exhibits a dependence on the chain length N, $E^* \sim N^{-1/2}$, which might be useful for electrophoretic separation of charged, collapsed biopolymers. For noncollapsed PEs this unfolding transition is less pronounced: the critical field depends on the swelling exponent ν and scales as $E^* \sim N^{-3\nu/2}$. The electrophoretic mobility of PE monomers and counterions is determined. For large fields, counterions bound to the PE contribute significantly to the total conduction, since they can glide along the PE. This is an important factor in understanding experimental conduction experiments. The electrophoretic mobility of the bound counterions is determined by the electrostatic friction with the PE backbone and an activation barrier for decondensing from the PE; it in fact changes sign as the field strength is increased.

I. Introduction

The behavior of polyelectrolytes (PE) exhibits a number of remarkable features that are due to the electrostatic coupling between polymeric and counterion degrees of freedom. Noteworthy is the sequence of PE conformations observed in simulations as the electrostatic coupling between the charges on the PE and the counterions is increased.[1−4] Experimentally, the coupling can be tuned by changing temperature, dielectric constant of the solvent, counterion valency, and size and charge density of the PE. For very small coupling the PE resembles a neutral polymer since the electrostatic repulsion between monomers is very small. As the coupling increases, the monomer−monomer repulsion leads to a more swollen configuration (the standard PE effect). However, as the coupling further increases, counterions condense on the PE and decrease the repulsion between monomers, and the PE starts to shrink. Finally, at very large electrostatic coupling, the PE is collapsed to a close-packed, almost charge-neutral condensate that contains most of its counterions. A similar sequence is experimentally seen with synthetic PEs[5] and DNA.[6−8] Of particular importance is the recently observed condensation of single DNA molecules,[8] since comparison with simulations of single PEs is possible.

All these phenomena concern the static, equilibrium behavior of PEs. In electrophoretic experiments, PEs are subject to external electric fields and the resulting mobility is measured.[9,10] Such techniques are widely used to separate DNA and charged proteins according to their molecular weight. In these situations, the electric field induces motion of ions and PEs, thus dissipation of energy, and one is facing a nonequilibrium problem. In this paper, we study the effects of electric fields on highly charged PEs using dynamical simulations and scaling arguments. In contrast to previous theories and simulations, where the counterions are not taken into account explicitly[11−13] or their coupling to the PE is rather weak,[14,15] we start from a strongly coupled PE−counterion system and investigate the resultant effects for large electric fields (i.e., far from equilibrium).[16]

We first analyze the static (zero-field) case and develop scaling arguments for the condensation of counterions on rodlike PEs and for the polarizability of a PE globule. Our simulations show that linear-response theory describes the induced dipole moment of a condensed PE globule in an electric field quantitatively up to a critical field strength at which the PE is oriented and straightened in the direction of the field. This nonequilibrium phenomenon occurs at a polarization energy equivalent to approximately thermal energy, which, together with our estimate of the polarizability of a PE globule, shows that the critical field strength scales as $E^* \sim N^{-1/2}$ with the polymer length N. Since one would expect the PE mobility to change drastically at the unfolding transition, this transition should be detectable by mobility measurements and in turn could be used for efficient separation of PEs of different length. In the more general case of a highly charged but noncollapsed PE characterized by a swelling exponent ν, the unfolding transition is less pronounced and occurs at a critical field strength $E^* \sim N^{-3\nu/2}$.

We in detail investigate the electrophoretic mobilities of the PE monomers, the bound counterions, and the unbound counterions. According to standard wisdom, a PE drags its condensed counterions along as it moves under the influence of an external electric field. We show this to be approximately correct only for very small fields and for strongly coupled PE−counterion systems. For large fields (of the order of the field strength needed to unfold or orient a PE), bound counterions start to glide along the PE and thus contribute considerably to the total conduction. Likewise, the PE electrophoretic mobility increases significantly at such electric fields. Since the characteristic field

† Part of the special issue "International Symposium on Polyelectrolytes".

10.1021/jp022618w CCC: $25.00
Published on Web 07/09/2003

strength needed to orient a PE chain is quite small for PEs with large monomer numbers, we expect these effects to be relevant for most experiments on free-solution PE electrophoresis.[9] Very recently, the mobility of DNA molecules adsorbed on cationic lipid bilayers was shown to increase with increasing field strength,[17] in rough agreement with our results. Similar effects are seen with highly charged dendrimers.[18]

Our results are obtained without hydrodynamic interactions. This is not problematic in the collapsed state, where solvent-mediated hydrodynamic interactions are overwhelmed by direct interactions between counterions and PE monomers (in fact, the water content of PE globules is quite low). In the field-aligned state and for lower coupling constants, hydrodynamic interactions are more important but will modify the main results only in a quantitative way (simulations that do include hydrodynamic interaction are on the way).[19]

II. Methods

In our dynamic simulations we consider a single PE chain consisting of N charged beads of valency q and radius a, in a cubic periodic box of length D together with N oppositely charged counterions of the same valency and radius. The box volume D^3 corresponds to the inverse PE concentration and plays an important role. We use the position Langevin equation, from which the velocity of the ith particle at time t follows as

$$\dot{\mathbf{r}}_i(t) = -\mu_0 \nabla_{\mathbf{r}_i} U(t) + \mu_0 q e s_i \mathbf{E} + \xi_i(t) \tag{1}$$

where μ_0 is the bare particle mobility (which is the same for counterions and monomers, as is appropriate since they have identical radii), U is the potential energy, $\mathbf{E}$ is the external electric field, and ξ_i is a vectorial random force acting on particle i. In the above expression, $s_i = -1$ for counterions and $s_i = 1$ for PE monomers. At the present stage of our theory we neglect hydrodynamic interactions between particles (as is justified since we are mostly interested in collapsed PEs where hydrodynamic forces are overwhelmed by electrostatic forces), and the random force is diagonal in the particles indices and correlated according to

$$\langle \xi_i(t) \xi_j(t') \rangle = 6 k_B T \mu_0 \delta(t - t') \delta_{ij} \tag{2}$$

In the simulations we discretize eq 1 with a time step Δ and rescale all lengths by the monomer/counterion radius a according to $\tilde{\mathbf{r}}_i = \mathbf{r}_i/a$. The iterative Langevin equation in terms of the discrete time variable $n = t/\Delta$ now reads

$$\tilde{\mathbf{r}}_i(n+1) = \tilde{\mathbf{r}}_i(n) - \tilde{\mu}_0 \nabla_{\tilde{\mathbf{r}}_i} \tilde{U}(n) + \tilde{\mu}_0 s_i \tilde{\mathbf{E}} + \sqrt{6\tilde{\mu}_0}\, \tilde{\xi}_i(n) \tag{3}$$

where $\tilde{U} = U/k_B T$ is the dimensionless potential energy, the rescaled electric field is

$$\tilde{\mathbf{E}} = q e a \mathbf{E}/k_B T \tag{4}$$

, and the rescaled random force has variance unity:

$$\langle \tilde{\xi}_i(m) \tilde{\xi}_j(n) \rangle = \delta_{mn} \delta_{ij} \tag{5}$$

The only parameter remaining is the rescaled mobility $\tilde{\mu}_0 = \Delta \mu_0 k_B T/a^2$, which is the diffusion constant in units of the particle radius a and time step Δ. In our simulations we chose $\tilde{\mu}_0 = 0.002$, which is a good compromise between efficiency and accuracy. The potential energy has several contributions:

$$\tilde{U} = \tilde{U}_c + \tilde{U}_{nn} + \tilde{U}_{LJ} \tag{6}$$

The Coulombic part is

$$\tilde{U}_c = \Xi \sum_{i<j} \frac{s_i s_j}{|\tilde{\mathbf{r}}_i - \tilde{\mathbf{r}}_j|} \tag{7}$$

where

$$\Xi = q^2 \ell_B / a \tag{8}$$

is the coupling strength and measures the ratio of the Coulomb interaction and the thermal energy at a typical distance a where $\ell_B = e^2/(4\pi\epsilon k_B T)$ is the Bjerrum length and denotes the distance at which two unit charges interact with thermal energy (in water, one has $\ell_B \approx 0.7$ nm). For most experimental polyelectrolyte systems, the distance between charges along the backbone is different from the distance of closest approach between PE charges and counterions. The present model is therefore a simplification where both parameters are merged into a single one. In comparing our results with experimental ones, we adopt the recipe of writing the linear charge density of a PE chain as $\tau = q/(2a)$, after which the coupling parameter becomes $\Xi = 2q\ell_B\tau$. For synthetic, fully charged vinyl-based PEs one has $\tau \approx 4$ nm^{-1} and thus $\Xi \approx 6q$; for DNA one has $\tau \approx 6$ nm^{-1} and thus $\Xi \approx 8q$. For mono- to trivalent counterions the coupling-parameter range of $\Xi \approx 5-30$ is therefore most relevant.

The connectivity of the PE is ensured by the term

$$\tilde{U}_{nn} = K \sum_{\langle ij \rangle} (|\tilde{\mathbf{r}}_i - \tilde{\mathbf{r}}_j| - 2)^2 \tag{9}$$

where the sum runs over nearest neighbors of the PE chain only. The bond stiffness is $K = 100$, which gives a very narrow distribution of bond lengths. Finally, collapse of counterions and charged monomers is prevented by a truncated Lennard-Jones term acting between all particles in the simulation:

$$\tilde{U}_{LJ} = \epsilon \sum_{i<j} \left(\frac{2^{12}}{(\tilde{\mathbf{r}}_i - \tilde{\mathbf{r}}_j)^{12}} - \frac{2^7}{(\tilde{\mathbf{r}}_i - \tilde{\mathbf{r}}_j)^6} + 1 \right) \tag{10}$$

used for separation $|\tilde{\mathbf{r}}_i - \tilde{\mathbf{r}}_j| < 2$ only with an energy parameter $\epsilon = 1$. Equilibration takes roughly 10^5 time steps; simulations were run for at least 10^7 time steps. Numerical errors are always of the order or smaller than the symbol sizes used. All results in finite electric fields have been obtained in the stationary state where all distribution functions are equilibrated. In all simulations we use periodic minimal-image boundary conditions, i.e., counterions and the PE can traverse the boundaries freely, but the minimal-image conditions prevent that the PE interacts with itself.

III. Static Behavior

In Figure 1 we show in the top panel a few snapshots of a PE chain with $N = 50$ monomers in the absence of an external field, exhibiting the well-known initial expansion of the chain due to increasing monomer−monomer repulsion (seen as one goes from $\Xi = 0$ to $\Xi = 1$), followed by a progressive condensation of counterions on the chain and concomitant collapse of the chain as the coupling parameter Ξ increases further.[1−4] This is reflected by the rescaled radius of gyration $\tilde{R}_g = R_g/a$ in Figure 1a, which shows for the various box sizes used a maximum at $\Xi \approx 3$.

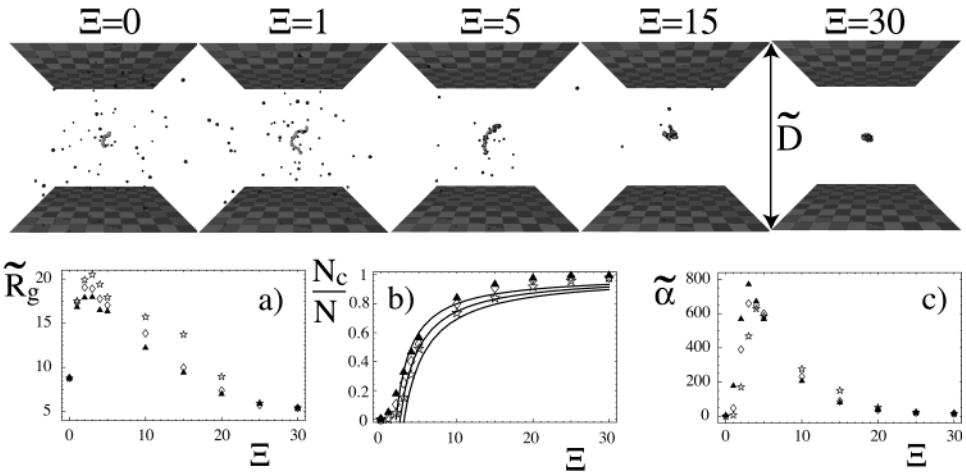

Figure 1. Simulation snapshots of a PE with $N = 50$ monomers and approximate length $\tilde{L} \approx 100$ in a cubic box of diameter $\tilde{D} = 200$ for various values of the coupling parameter Ξ. (a) Radius of gyration $\tilde{R}_g$, (b) average rescaled number of condensed counterions N_c/N, and (c) polarizability $\tilde{\alpha}$ for a PE of monomer number $N = 50$ and box sizes $\tilde{D} = 400$ (☆), $\tilde{D} = 200$ (◇), and $\tilde{D} = 100$ (▲).

The radius of gyration of the PE is defined as

$$\tilde{R}_g{}^2 = \frac{1}{2N^2}\sum_{i,j=1}^{N}\langle(\tilde{r}_i - \tilde{r}_j)^2\rangle = \frac{1}{N}\sum_{i=1}^{N}\langle(\tilde{r}_i - \tilde{R}_{com})^2\rangle \quad (11)$$

where the sum includes PE monomers only and $\tilde{R}_{com}$ denotes the center of mass in rescaled coordinates defined as

$$\tilde{R}_{com} = \frac{1}{N}\sum_{i=1}^{N}\tilde{r}_i \quad (12)$$

There is a systematic trend in the data showing that the radius of gyration is larger for larger box sizes. This can be understood by studying the degree of counterion condensation. The number of condensed counterions (rescaled by the total number of counterions), N_c/N, is shown in Figure 1b and depends weakly on the box size: the bigger the box, the smaller the number of condensed counterions. Throughout this paper, we rather arbitrarily defined a counterion as condensed when its center is closer than $4a$ to any monomer center, i.e., when there is at least one monomer closer than 2 times the diameter (we checked that our results depend only very weakly on the precise distance chosen to discriminate between condensed and uncondensed counterions). Since the number of condensed counterions goes down with increasing box size, it is fairly easy to understand that the effective PE repulsion goes up and thus the radius of gyration increases. But why is the counterion condensation depending on box size in the first place? The simplest approach toward counterion condensation on finite-size cylinders[20] starts with the observation that the electrostatic energy of an infinitely long cylindrical capacitor of inner radius a, outer radius H, and linear charge density $q/2a$ is given per unit length and in units of k_BT by $w = \Xi \ln(H/a)/4a$. The electrostatic self-energy of a cylinder of finite length L (embedded in a box much larger than its length, $D \gg L$) can be decomposed into the self-energy of its electric near field (at distances from the cylinder surface smaller than L) and its far field (at distances larger than L). In the near-field region, the electric field distribution is almost like that of the cylindrical capacitor and we thus replace, in the expression for the cylindrical capacitor energy, the outer radius H by the polymer length L and obtain the energy contribution per unit length $w \simeq \Xi \ln(L/a)/4a$; the far-field distribution is almost like that of a pointlike charged object and we obtain the self-energy (per unit length) $w \sim \Xi/a$, which is of subleading order and can therefore be neglected. It is important to note that the cylinder self-energy does not depend on the box size to leading order (this holds given that the box size is larger than the cylinder length, which is always the case in our simulations). Assuming that a fraction x of counterions condenses on the cylinder, the modified electrostatic energy becomes

$$w \simeq (1 - x)^2\,\Xi \ln(L/a)/4a \quad (13)$$

Details of the counterion distribution, e.g., their mean distance from the inner cylinder, only influence the next-leading order and are therefore irrelevant for the present arguments. The entropy cost of confining a fraction x of counterions from the uncondensed state (where they are assumed to be homogeneously distributed within the box of volume D^3) into a cylindrical compartment of approximate volume $\approx La^2$ scales (per unit length) as

$$s \simeq x \ln(D^3/La^2)/2a \quad (14)$$

Minimizing the total free energy $w + s$ with respect to x, the fraction of condensed ions, one obtains the leading result for large L/a and D/L:

$$x = 1 - \frac{2}{\Xi}\left(1 + \frac{3\ln(D/L)}{2\ln(L/a)}\right) \quad (15)$$

which is shown in Figure 1b as solid lines for the three different box sizes used. The agreement between this simple theory and the simulations is quite satisfactory; it should be kept in mind that the precise number of condensed counterions depends on our definition used and one should therefore concentrate on the qualitative aspects. For infinitely long cylinders $L/a = \infty$, the exact Manning limit $x = 1 - (2/\Xi)$ with the condensation threshold at $\Xi^* = 2$ is recovered,[21] which corresponds to the upper solid line in Figure 1b, but for finite-length cylinders an increasing box size D/L indeed decreases the number of condensed ions, in agreement with our simulation results.

Figure 2 shows numerical data for the number of condensed ions for fixed coupling strength $\Xi = 10$ and a variety of different chain lengths and box sizes: for monomer number $N = 50$ ($L/a = 100$) and box sizes $D/L = 4$ (☆), $D/L = 2$ (◇), and $D/L = 1$ (▲); for $N = 25$ ($L/a = 50$) and $D/L = 2$ (□); and for $N = 100$ ($L/a = 200$) and $D/L = 2$ (■). The asymptotic prediction (eq 15) for $L/a = 100$ is shown as a broken line. The logarithmic

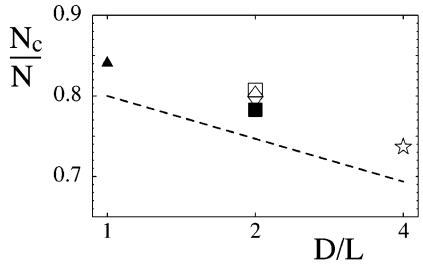

Figure 2. Comparison of the rescaled number of condensed counterions N_c/N for fixed coupling strength $\Xi = 10$ and different polymer lengths and box sizes in a semilogarithmic plot. Data are shown for $N = 50$ ($\tilde{L} \approx 100$) and box sizes $\tilde{D} = 400$ (☆), $\tilde{D} = 200$ (◇), $\tilde{D} = 100$ (▲), for $N = 25$ ($\tilde{L} \approx 50$) and $\tilde{D} = 100$ (□), and for $N = 100$ ($\tilde{L} \approx 200$) and $\tilde{D} = 400$ (■).

dependence on the relative box size D/L is captured quite well by the simulation data. In agreement with the analytic prediction, the dependence on the chain length L/a is much weaker (since the absolute value L/a is much larger and thus a relative increase by a factor of 4 plays less a role) and all three data points for $D/L = 2$ agree within the numerical error (which is on the order of the symbol size). The overall agreement between scaling prediction and simulation is somewhat surprising, since the PE is not a straight cylinder and one is far from the asymptotic limit of large L/a and D/L. A similar calculation for spherical condensates predicts a phase transition from the cylindrical to the spherical condensate for a characteristic value of Ξ.[22,19]

The rescaled dipole moment of the PE with its counterions is given by

$$\tilde{\mathbf{P}} = \sum_i s_i(\tilde{\mathbf{r}}_i - \tilde{\mathbf{R}}_{\text{com}}) \tag{16}$$

where the sum includes all PE monomers and only those counterions that are condensed (using the same definition as previously for Figure 1b) on the PE. The origin $\tilde{\mathbf{R}}_{\text{com}}$ is chosen to be the center of mass of the PE (since the PE−counterion complex has a net charge, the precise value of the dipole moment does depend on the choice of origin). In Figure 1c the polarizability according to the fluctuation−dissipation theorem

$$\tilde{\alpha} = k_B T\alpha/(qea)^2 = \langle \tilde{P}^2 \rangle/3 \tag{17}$$

is shown. The resultant polarizability shows a strong Ξ dependence and qualitatively follows the trend of the radius of gyration shown in Figure 1a. The classical result for the polarizability of a sphere with radius R and uniformly distributed charge Q around an opposite point charge Q' is for $Q = Q'$ given by $\alpha = 4\pi\epsilon R^3$ [23] or, in rescaled units, $\tilde{\alpha} = \tilde{R}^3/\Xi$. Identical results are obtained from the Clausius−Mosotti equation or with different, more complicated charge distributions. For a system with a net charge, $Q < Q'$, the polarizability (measured with respect to the center of the charge distribution Q', similarly to our analysis of the simulation data) is reduced:

$$\tilde{\alpha} = \frac{Q\tilde{R}^3}{\Xi Q'} = \frac{N_c\tilde{R}^3}{\Xi N} \tag{18}$$

which can be easily understood since now the electrostatic force that counteracts the displacement of the spherical charge distribution $Q = N_c$, corresponding to the condensed counterions, due to the external field is stronger. Accordingly, we replot in Figure 3 the data for $\tilde{D} = 200$ from Figure 1c as $(\tilde{\alpha}N/N_c)^{1/3}$ versus $\tilde{R}_g/\Xi^{1/3}$ together with the prediction of eq 18, which is a straight line of slope unity. (Note that in the scaling plot the

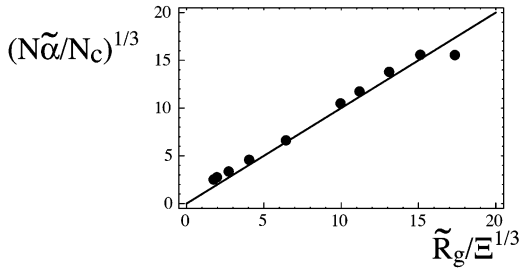

Figure 3. Parametric scaling plot of the polarizability $\tilde{\alpha}$ for a PE with $N = 50$ monomers in a box of size $\tilde{D} = 200$ for different values of Ξ. The data follow closely the prediction of eq 18, shown as a solid line, meaning that indeed $\tilde{\alpha} \simeq N_c\tilde{R}_g^3/N\Xi$ within high precision regardless of the value of Ξ.

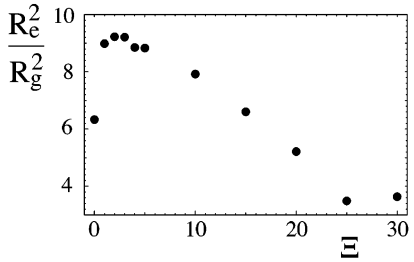

Figure 4. Ratio of the polymer squared end-to-end radius R_e^2 and the squared radius of gyration R_g^2 for a PE with $N = 50$ monomers in a box of size $\tilde{D} = 200$.

value of Ξ decreases as one goes from the left to the right and all numerical data from $\Xi = 1$ to $\Xi = 30$ are shown.) The good agreement demonstrates that our simple scaling model allows a quantitative description of the PE polarizability even for situations where the PE structure is quite elongated and thus deviates from a spherical charge distribution used in deriving eq 18. We will see in a later section that the scaling prediction for the polarizability of a chain is also useful to predict the PE response to an external electric field.

The evolution of PE shape with increasing coupling constant Ξ is best appreciated from Figure 4 where the ratio of the mean squared end-to-end distance R_e^2 defined by

$$\tilde{R}_e^{\,2} = \langle (\tilde{r}_1 - \tilde{r}_N)^2 \rangle \tag{19}$$

and the mean squared radius of gyration R_g^2 defined in eq 11 is shown. For an ideal Gaussian chain one expects $R_e^2/R_g^2 = 6$, for a self-avoiding chain one finds $R_e^2/R_g^2 \approx 6.33$ (close to what we observe for $\Xi = 0$ in the absence of electrostatic interactions) and for a stiff rod one has $R_e^2/R_g^2 = 12$. The maximal ratio in our simulation is about $R_e^2/R_g^2 \approx 9.5$, which is close to what had been observed in previous simulations.[1] How the rodlike behavior is approached in the limit of an infinitely long chain depends in a subtle way on how the box size is increased while the chain length grows. An inspection of eq 15 shows that when the box size/polymer length ratio D/L is kept fixed in the infinite-chain limit $L/a \to \infty$, the condensation of counterions is maximal and the chain is effectively quite weakly charged. The limit of a stiff rod will be approached quite slowly. If on the other hand the relative box size D/L is increased more rapidly than the polymer length L/a, counterion condensation will be inhibited. The chain will regain its bare charge and the stiff-rod limit will be approached more rapidly. In a collapsed globule and in the limit of a very long chain, the mean-squared monomer−monomer distance becomes independent of the monomer−monomer distance along the contour of the chain. It follows directly from the definition of the radius of gyration in eq 11

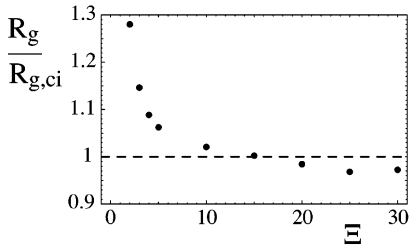

Figure 5. Ratio of the polymeric radius of gyration R_g and the counterion radius of gyration $R_{g,ci}$ for a PE with $N = 50$ monomers in a box of size $\tilde{D} = 200$.

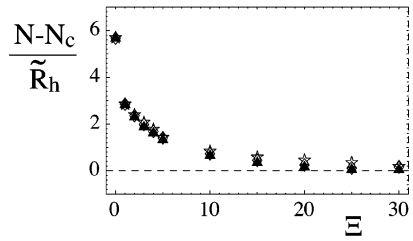

Figure 6. Ratio of the effective complex charge, $N - N_c$, and the hydrodynamic radius, $\tilde{R}_h$, for a PE with $N = 50$ monomers in a box of size $\tilde{D} = 200$. This ratio is an estimate for the effective electrophoretic mobility of a PE chain including hydrodynamic effects.

that the squared radius of gyration becomes $\tilde{R}_g^2 = \tilde{R}_e^2/2$ in that limit. In Figure 4 we observe indeed that the characteristic ratio becomes increasingly smaller for large coupling constants, but we are still quite far from the expected ratio $R_e^2/R_g^2 = 2$. The reason for this is supposedly that our chains are quite short and that the equilibration time becomes very long in the collapsed phase.

To understand the structure of the PE−counterion complex, one also needs to characterize the counterion distribution. One way of doing this is to look at the counterion radius of gyration, which is defined in analogy to the PE radius of gyration, eq 11, but summing over condensed counterions instead. In Figure 5 we show the ratio of the polymeric radius of gyration R_g and the counterion radius of gyration $R_{g,ci}$ (calculated only with those counterions that are condensed according to the criterion used before). As can be seen, for small values of the coupling constant this ratio is larger than unity; that means the counterions are concentrated toward the center of the PE. This can be easily understood, since in the extreme case of a single condensed ion it is clear that this ion will be electrostatically drawn toward the center of the PE. As more and more counterions condense on the PE, the data show that this ratio becomes eventually smaller than unity, i.e., the counterion distribution is more diffuse than the PE distribution. This is also not hard to understand, since the counterion distribution is not bounded at large distances (unlike the PE distribution function) and there is always a certain nonzero probability of finding a counterion at a certain distance away from the PE center.

Experimentally, the electrophoretic mobility of DNA has been measured as a function of spermidine concentration and found to decrease dramatically.[8] This is somewhat surprising, since spermidine (a trivalent counterion) induces collapse of the DNA, decreases the radius of the DNA coil, and therefore lowers the hydrodynamic friction. However, the electrophoretic mobility μ_{el} is the ratio of the effective charge and the friction coefficient, and since the effective charge goes down as the DNA is compacted, it is not clear in which direction the electrophoretic mobility changes. In Figure 6 we plot the ratio of the effective complex charge and hydrodynamic radius $(N - N_c)/\tilde{R}_h$, which is a quite reliable estimate for the electrophoretic mobility.[14] The hydrodynamic radius is given by[24]

$$\tilde{R}_h^{-1} = \frac{1}{N^2} \sum_{i \neq j} \langle |\tilde{r}_i - \tilde{r}_j|^{-1} \rangle \tag{20}$$

As our simulations show, the electrophoretic mobility indeed goes down with progressing compaction, in agreement with the experimental results for DNA collapsed with spermidine.[8] This means that the decrease of the effective charge dominates the decrease of the hydrodynamic radius. It is at present not clear whether this result is universally valid for different experimental realizations (e.g., collapse induced by changing the dielectric constant of the solvent, different types of condensing agents) and how the stiffness of the DNA, which is not included at the present level of our theory, will come into play.

IV. Dynamic Behavior in the Collapsed Phase

In the following sections we study the behavior of the PE complex under the action of an external electric field. An external field leads to dissipation of energy and therefore shifts the system away from equilibrium. For small fields, linear-response theory will be valid and equilibrium (zero-field) distribution functions will only be slightly perturbed. For large fields, however, we observe pronounced departure from the equilibrium behavior. In this section we consider a coupling constant of $\Xi = 20$, i.e., we concentrate on the strongly collapsed case. Figure 7 shows a few snapshots for increasing field strength, exhibiting an unfolding transition of the PE condensate at a critical field strength.

The nonequilibrium unfolding transition manifests itself as a rather abrupt increase of the rescaled end-to-end radius $\tilde{R}_e/\tilde{L}$, which in Figure 7a is shown for $\Xi = 20$ and various box sizes as a function of the applied field. The number of condensed counterions in the high-field extended configuration exhibits a dramatic dependence on the box size (see Figure 7b). It approximately equals the ratio of polymer length and box size, $N_c/N \approx \tilde{L}/\tilde{D}$, since the counterions in the large-electric-field limit are distributed almost evenly along the electric-field direction. The electrophoretic mobility of a charged counterion or PE monomer is defined as

$$\tilde{\boldsymbol{\mu}} = \boldsymbol{s}_i \langle \tilde{\mathbf{r}}(n+1) - \tilde{\mathbf{r}}(n) \rangle / \tilde{E} \tag{21}$$

and is equivalent to the conductivity. In the absence of interactions between PE monomers and counterions, or in the limit of infinite dilution, the electrophoretic mobility equals the bare mobility $\tilde{\mu}_0$ for all charged particles. In Figure 7c we show the PE monomer mobility for different box sizes as a function of the external field. For small fields the mobility is almost zero, i.e., the condensed counterions slow the PE considerably (we will later account for this limiting behavior in a quantitative fashion). As the field strength increases, the rescaled mobility $\tilde{\mu}/\tilde{\mu}_0$ slowly approaches unity. This is an extreme example of a Wien effect,[25] which has originally been observed for simple electrolyte solutions. As the external driving field increases, i.e., as one moves further away from equilibrium, the system changes its distribution functions and maximizes the dissipation. Similar effects have previously been studied in the context of driven lattice-gas models.[26−28] Since the characteristic electric field needed to orient the PE goes down with increasing monomer number, this effect is quite relevant for experimental situations, as we will discuss later on. It is interesting to note that the mobility shows a much less abrupt behavior close to the critical

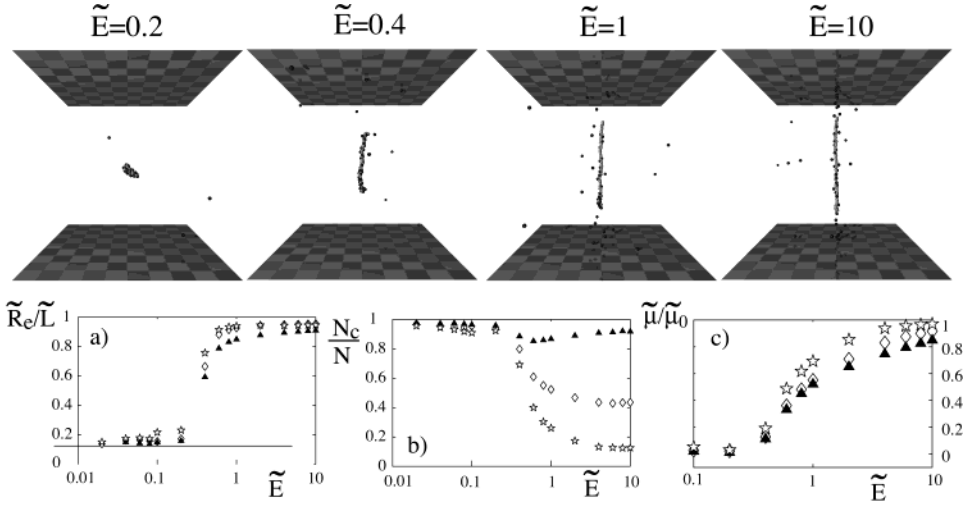

Figure 7. PE snapshots for fixed coupling constant $\Xi = 20$ and box size $\tilde{D} = 200$ and various rescaled field strengths, exhibiting an unfolding transition at $\tilde{E} \approx 0.2$. (a) End-to-end radius $\tilde{R}_e/\tilde{L}$, (b) number of condensed counterions N_c/N, and (c) mobility of PE monomers for a PE of length $\tilde{L} = 100$ and box sizes $\tilde{D} = 400$ (☆), $\tilde{D} = 200$ (◇), and $\tilde{D} = 100$ (▲) for $\Xi = 20$.

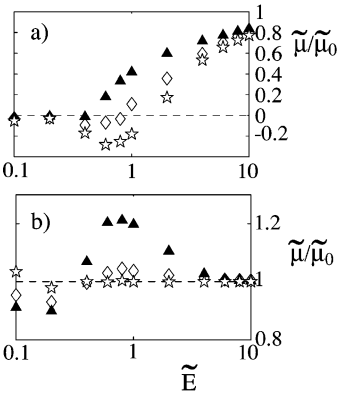

Figure 8. Mobility for (a) condensed and (b) uncondensed counterions at a coupling $\Xi = 20$ for a PE of length $\tilde{L} = 100$ and box sizes $\tilde{D} = 400$ (☆), $\tilde{D} = 200$ (◇), and $\tilde{D} = 100$ (▲).

field, as for example the end-to-end radius in Figure 7a or the number of condensed counterions in Figure 7b.

In Figure 8 we present the mobility of condensed counterions (panel a) and uncondensed counterions (panel b) as a function of the external field (with the same criterion for discriminating between the two classes of counterions as used in Figure 1b). As can be seen, the mobility of condensed counterions is negative for small fields: the counterions are dragged along with the PE. This is in accord with a theoretical model that was used to desribe experimental conduction data of highly charged PEs.[29] However, as the field strength increases, their mobility changes sign. For large fields, the mobility is positive and the counterions thus glide along the PE. This behavior has not been considered before, and we believe this gliding to be important to correctly interpret conduction experiments on PEs in free solution.

It is important to note that the mobility of condensed counterions depends a lot on the box size at intermediate field strengths: the smaller the box size, the larger the mobility. Two factors determine the mobility of condensed counterions: (i) the *electrostatic friction* between a moving counterion and the inhomogeneously charged PE backbone that moves in the opposite direction and (ii) the *asymmetry field* or *relaxation field* due to the asymmetric distribution of condensed counterions along the PE, which counteracts the external electric field.[14] A different, equivalent interpretation is to say that counterions that are bound to the PE have an activation barrier to overcome before they can decondense and move along their preferred field direction. Since the continuity equation demands that for a stationary state (which we always consider) the rate at which counterions decondense from the PE equals the flux of condensed and also the flux of decondensed ions, one sees that these different points of view are not independent. The asymmetry field depends sensitively on the box size. The extreme case is a PE that has the same length as the box and therefore spans the periodic box (our results for $\tilde{D} = 100$, ▲ in Figure 8, are close to this limit). In this case, there is almost no asymmetry field and the reduced mobility is mostly due to electrostatic friction between the PE and the condensed counterions. In contrast to the condensed ions, the mobility of the uncondensed counterions is only weakly varying and of the order of unity. The overshoot for a box size $\tilde{D} = 100$ (▲ in Figure 8b) is a signature of the weak asymmetry field acting between the polymer ends, which tends to accelerate the counterions in the interstitial space between the two ends.

In Figure 9a we compare the average mobility of PE monomers (◇) with the average mobility of all counterions (condensed and uncondensed, ■) for a box size $\tilde{D} = 200$. Not surprisingly, the two are the same within numerical error, which reflects a fundamental symmetry of our model: since the total charges of monomers and counterions are the same, the total force due to the external electric field on counterions and monomers is the same. On average, the internal forces also balance. Since the bare mobilities are assumed to be the same, the effective mobilities are the same, as indeed seen in Figure 9a. With the effective mobilities of monomers, condensed counterions, and uncondensed counterions denoted respectively by $\tilde{\mu}_m$, $\tilde{\mu}_c$, and $\tilde{\mu}_u$, this force equilibrium condition can be written as

$$N\tilde{\mu}_m = N_c\tilde{\mu}_c + (N - N_c)\tilde{\mu}_u \qquad (22)$$

The mobility of the condensed counterions and the PE monomers is very small at low fields, mostly because the condensate is almost charge-neutral; this effect is due to strong electrostatic friction within the collapsed globule. Assuming the effective mobility of monomers and condensed counterions to be proportional to the ratio of the effective charge, $N - N_c$, and

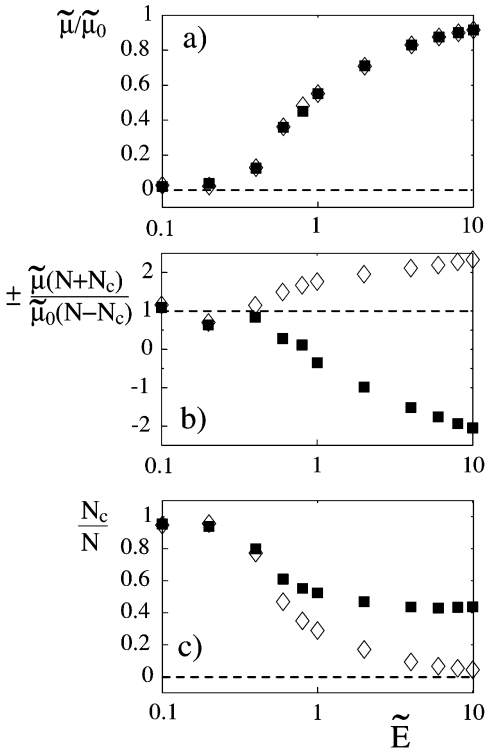

Figure 9. More detailed analysis of mobility results for a chain of length $\tilde{L} = 100$ in a box of size $\tilde{D} = 200$ at a coupling constant $\Xi = 20$. (a) Mobility of PE monomers (◊) compared with the average mobility of all counterions, condensed and uncondensed (■). (b) Rescaled monomer mobility (+, ◊) and condensed counterion mobility (−, ■). (c) Number of condensed counterions as measured in the simulation (■, same data as shown in Figure 7b) compared with the prediction from the PE mobility assuming tight binding (◊).

the total number of particles in the globule (i.e., the effective friction coefficient), $N + N_c$, the prediction for the mobilities is

$$\tilde{\mu}_m = -\tilde{\mu}_c = \frac{N - N_c}{N + N_c}\tilde{\mu}_0 \tag{23}$$

which corresponds to the tight-binding limit. Accordingly, we plot in Figure 9b the rescaled mobilities of monomers and counterions, which according to the prediction of eq 23 should be unity. Indeed, for smaller fields the data are close to unity, which shows that the effective mobility of the collapsed globule is mostly dominated by its effective charge and that condensed counterions are completely dragged along with the globule. For larger fields the counterions start to migrate in their proper direction, and the mobility of condensed counterions changes sign.

Is the low-field strong-friction prediction of eq 23 compatible with the force-balance of eq 22? In fact, combining both equations, one finds $\tilde{\mu}_u = \tilde{\mu}_0$; that is, the uncondensed counterions follow to have a mobility corresponding to their bare mobility. This also means that the deviations we see in Figure 9b from the predictions in eq 23 (corresponding to a rescaled mobility of unity) do have their counterpart in equal deviations of the uncondensed counterion mobility from the bare mobility (as indeed seen in Figure 8b).

The prediction for the PE monomer mobility, eq 23, can be inverted to obtain the number of condensed counterions as a function of the PE mobility, leading to

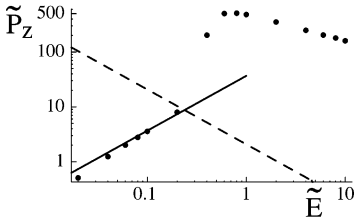

Figure 10. Induced dipole moment $\tilde{P}_z$ for $\Xi = 20$ and $\tilde{D} = 200$ as a function of the rescaled field $\tilde{E}$. The linear-response prediction, $\tilde{P} = \tilde{\alpha}\tilde{E}$ (−), and its limit of validity, $\tilde{P} = 2/\tilde{E}$ (− − −), are shown.

$$\frac{N_c}{N} = \frac{1 - (\tilde{\mu}_m/\tilde{\mu}_0)}{1 + (\tilde{\mu}_m/\tilde{\mu}_0)} \tag{24}$$

In Figure 9c we show the predicted number of condensed counterions according to eq 24 (◊) together with the number of condensed counterions actually determined in the simulations (by the same criterion as in Figure 1b; ■). The tight binding prediction, eqs 23 and 24, performs quite well for small fields but underestimates the number of condensed counterions for large fields since it does not account for the relative motion of monomers and condensed counterions (i.e., counterion gliding), which is the dominant mode of motion at large fields. Overall, the mobility of PE globules, which is a measure of dynamic counterion binding, gives results that are for small fields in quantitative agreement with the static counterion-binding predictions.

In Figure 10 we plot the *z*-component of the dipole moment of the PE and its condensed counterion cloud for a box size $\tilde{D} = 200$. The solid line is the linear-response prediction $P = \alpha E$ or, in rescaled coordinates, $\tilde{P} = \tilde{\alpha}\tilde{E}$, with $\tilde{\alpha} = 36.7$ taken from the static simulation data (Figure 1c). The broken line denotes the threshold where the rescaled polarization energy $W_{pol}/k_BT = PE/2k_BT = \tilde{P}\tilde{E}/2$ reaches unity, i.e., $\tilde{P} = 2/\tilde{E}$.

At this threshold the electric field is strong enough to orient the spontaneous dipole moment of the PE globule and to excite soft deformation modes: linear-response theory is expected to break down. [Also, nonequilibrium effects are expected to be important at large electric fields. However, it is difficult to clearly separate equilibrium from nonequilibrium effects. In principle, an electric field in the absence of conduction (dissipation) would lead to similar effects, but such a scenario is impossible to study.] As the data show, this threshold indeed denotes the onset where the PE globule starts to unfold. Combining the expression for the unfolding field strength, $\tilde{E}^* = (\tilde{\alpha}/2)^{-1/2}$ (as follows from the condition $W_{pol}/k_BT = \tilde{\alpha}\tilde{E}^2/2 = 1$), our previously demonstrated result for the polarizability of a nearly-neutral globule, $\tilde{\alpha} = \tilde{R}_g^3/\Xi$, and the scaling of a compact globule, $\tilde{R}_g^3 \simeq N$, we finally obtain $\tilde{E}^* \simeq (\Xi/N)^{1/2}$ or, in nonrescaled units, $eE^* \simeq k_BT(a^3N/\ell_B)^{-1/2}$. This shows that the unfolding field strength depends on the polymer length, which could be used for electrophoretic separation studies of long PEs, which are collapsed with some condensing agent: since the mobility is expected to change drastically with the unfolding, at a suitably chosen field strength a rather sensitive size discrimination should be possible since the longest PEs will have unfolded while the shorter ones are still collapsed.

A reduced electric field corresponding to the unfolding transition, $\tilde{E} = 0.2$, corresponds for a monomer/counterion radius $a = 0.25$ nm and divalent ions ($q = 2$) to a field of $E \simeq 10^7$ V/m. Extrapolating our result for $N = 50$ to longer PEs, we expect the unfolding to occur at $E \simeq 10^6$ V/m for $N = 5 \times$

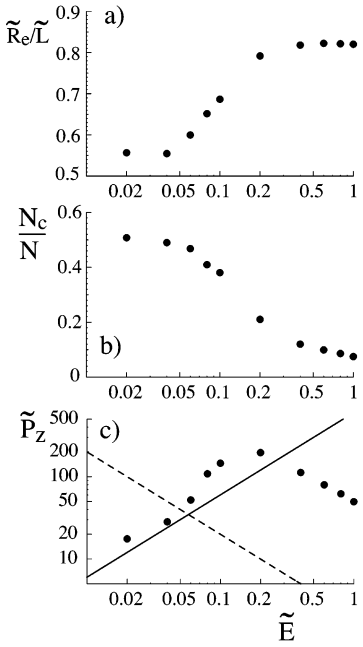

Figure 11. Data for fixed coupling constant $\Xi = 5$ and box size $\tilde{D} = 200$ as a function of the rescaled field strength, exhibiting a weak unfolding transition starting at $\tilde{E} \approx 0.05$. (a) End-to-end radius divided by mean polymer length, $\tilde{R}_e/\tilde{L}$, (b) relative number of condensed counterions N_c/N, and (c) induced rescaled dipole moment $\tilde{P}_z$. The linear-response prediction, $\tilde{P} = \tilde{\alpha}\tilde{E}$ (—), and its limit of validity, $\tilde{P} = 2/\tilde{E}$ (— — —), are shown.

10^3 and at $E \simeq 10^5$ V/m for $N = 5 \times 10^5$, which are feasible values for capillary experiments.

V. Dynamic Behavior in the Noncollapsed Phase

In this section we study the behavior of a noncollapsed PE−counterion system characterized by a coupling constant $\Xi = 5$, which roughly corresponds to a synthetic polymer with one charge every 0.3 nm (which is close to vinyl-based fully charged polyelectrolytes) and monovalent counterions.

In Figure 11a we show the rescaled mean end-to-end radius as a function of the external field. It is important to note that a PE characterized by a coupling constant $\Xi = 5$ is at low fields in a state intermediate between a collapsed and a stretched state (see Figure 1). Although the PE is not collapsed at zero field, the data exhibit the signature of a weak unfolding transition which starts at a critical field strength of $\tilde{E}^* \simeq 0.05$. At the same field strength, the number of condensed counterions starts to decrease (the hypthetical fraction of condensed counterions in the infinite-chain limit according to eq 15 would be $N_c/N = 0.6$), as can be seen in Figure 11b. Figure 11c shows the dipole moment of the PE with its condensed counterions, together with the linear-response prediction based on polarizability data shown in Figure 1c (solid line) and the expected threshold of orientation at which the polarization free energy equals thermal energy (broken line). Even for this noncollapsed polymer, the polarizability is quite well described by the spherical charge-cloud model discussed before. The simple criterion for the onset of the unfolding transition is surprisingly accurate and allows us to quantitatively estimate the characteristic unfolding/orientation field strength.

A reduced electric field corresponding to the unfolding transition, $\tilde{E} = 0.05$, corresponds for a monomer/counterion radius $a = 0.25$ nm and monovalent ions ($q = 1$) to a field of $E \simeq 5 \times 10^6$ V/m. In the general case of an uncollapsed PE chain we can generalize our scaling model for the unfolding transition in the following way. We again combine the expression for the unfolding field strength, $\tilde{E}^* = (\tilde{\alpha}/2)^{-1/2}$ (which follows from the condition $W_{pol}/k_BT = \tilde{\alpha}\tilde{E}^2/2 = 1$), with the result for the polarizability of a PE chain, $\tilde{\alpha} = N_c\tilde{R}_g^3/(N\Xi)$, and the scaling of the radius of gyration, $\tilde{R}_g \simeq (\ell/a)(Na/\ell)^\nu$. The persistence length of the chain is denoted by ℓ and in principle will depend on the ambient salt concentration. The swelling exponent varies between $\nu = 1$ in the rodlike phase (obtained at extremely low salt concentrations at length scales up to the persistence length) and $\nu = {}^1/_3$ in the collapsed phase. We obtain for the critical unfolding field

$$\tilde{E}^* \simeq \left(\frac{N\Xi}{N_c}\right)^{1/2}\left(\frac{a}{\ell}\right)^{3(1-\nu)/2} N^{-3\nu/2} \tag{25}$$

or in nonrescaled units

$$\frac{eE^*}{k_BT} \simeq \left(\frac{N\ell_B}{N_c a^3}\right)^{1/2}\left(\frac{a}{\ell}\right)^{3(1-\nu)/2} N^{-3\nu/2} \tag{26}$$

The previous results in the collapsed phase are obtained by setting $\nu = {}^1/_3$ and $N_c = N$. Extrapolating our result for $N = 50$ to longer PEs, for a fully stretched PE with a swelling exponent $\nu = 1$, we expect the unfolding to occur at $E \simeq 5 \times 10^3$ V/m for $N = 5 \times 10^3$ and at $E \simeq 5$ V/m for $N = 5 \times 10^5$. These are very small field strengths, and it follows that long PEs in the absence of added salt will be unfolded even at moderate field strengths. In the presence of salt the swelling exponent will be eventually (at large scales) given by the good-solvent exponent $\nu \approx {}^3/_5$ and the unfolding will occur for slightly longer chains. The unfolding/orientation transition is therefore observable in experimental situations, and it is probably one of the explanations for the observed free-draining behavior of charged polymers. Indeed, it is known from DNA measurements that the electrophoretic mobility becomes independent of chain length above a certain threshold, which for a field strength of approximately 10^4 V/m is $N \simeq 200$,[9] roughly of the same order as our estimates. We mention that the unfolding and alignment of DNA molecules adsorbed on oppositely charged membranes,[17] on mica surfaces,[30] and in free solution[31,32] in large electric fields has recently been observed experimentally by optical imaging techniques. Similar effects are also seen with much stiffer actin molecules.[33] The critical fields have yet to be determined. The orientation of flexible synthetic PEs in solution can be quantified by electric birefringence techniques,[34] where the employed field strengths are typically smaller than those needed to fully orient the chains.

In Figure 12a we show the mobility of PE monomers and condensed and uncondensed counterions as a function of the field. A number of differences from the collapsed case shown in Figures 7 and 8 are apparent. The mobilities of monomers and condensed counterions saturate at a finite value quite different from zero for small fields. The mobility of uncondensed counterions (☆) is quite different from unity, so there is substantial interaction between uncondensed ions and the complexes. In agreement with our previous discussion, bound counterions (▲) are dragged along with the PE for small fields but start to reverse their mean direction of motion as the field increases. In Figure 12b we plot the rescaled mobilities of monomers and counterions, which according to the prediction of eq 23 should be unity. For smaller fields the data are somewhat close to unity, which shows that the effective mobility of the PE chain can be within a fair approximation described by its effective charge. According to our discussion after eq

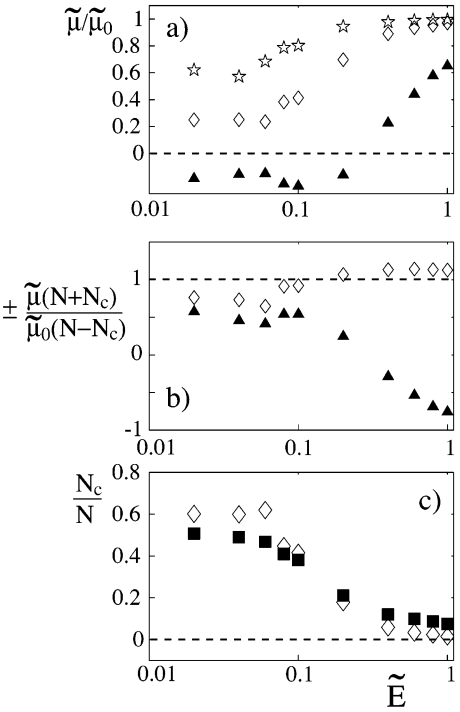

Figure 12. Data for a PE of length $\tilde{L} = 100$ and fixed coupling constant $\Xi = 5$ and box size $\tilde{D} = 200$ at various rescaled field strengths. (a) Mobility for PE monomers (◊), condensed counterions (▲) and uncondensed counterions (☆). (b) Rescaled monomer mobility (◊, +) and condensed counterion mobility (▲, −), which according to the tight-binding prediction eq 23 should be unity. (c) Number of condensed counterions as actually measured in the simulation (■) compared with the prediction from the PE mobility assuming tight binding (◊).

23, the deviations we see in Figure 12b from unity are linked to the deviations of the uncondensed counterion mobility from unity as seen in Figure 12a.

For larger fields the counterions start to migrate in their proper direction, and the condensed-counterion mobility changes sign. In Figure 12c we show the predicted number of condensed counterions according to the tight-binding approximation, eq 24 (◊), together with the number of condensed counterions actually determined in the simulations (■). The tight-binding prediction performs quite well for small fields; it in fact gives an estimate of the number of condensed counterion closer to the asymptotic Manning prediction $N_c/N = 0.6$ than our direct estimate, which of course depends on the arbitrary geometric distinction between condensed and uncondensed counterions; in contrast to that, the dynamic definition of condensed counterions does not depend on any definition. Both estimates for the number of condensed ions go down with increasing field strength, which on one hand reflects that the field ionizes the PE. On the other hand, it is clear from Figure 12c that the prediction of eq 24 underestimates the number of condensed counterions for large fields. The reason is that it does not account for the relative motion of monomers and condensed counterions.

VI. Discussion

We have investigated in detail the behavior of a single charged polymer in electric fields using Brownian dynamics simulations and scaling arguments. In the simulations we have included the counterions explicitly, to prevent evaporation of counterions we have enclosed the PE in a periodic box. In the absence of an electric field we have tuned the electrostatic coupling parameter Ξ in a wide range and recovered the previously known sequence of PE stretching, counterion condensation, and PE collapse as the coupling increases. We then turned on the electric field and observed that, starting from a strongly collapsed state for $\Xi = 20$ (which experimentally can be reached by adding multivalent counterions to, e.g., DNA), the field induces an unfolding and orientation transition at a characteristic field strength $\tilde{E}^*$. This transition contains a dissipation-driven nonequilibrium component that tends to maximize the entropy production. However, it is difficult to say exactly how much of the observed effect is due to the nonquilibrium (dissipation-driven) mechanism and how much is due to the equilibrium polarization effect. Scaling arguments (backed up by our simulations) predict the characteristic field strength to scale as $\tilde{E}^* \sim N^{-3\nu/2}$ with the PE length N, where ν is the swelling exponent, which varies between $\nu = {}^1/_3$ for collapsed PE globules and $\nu = 1$ in the salt-free expanded case. PEs of different lengths therefore unfold at different field strengths, a phenomenon that opens the possibility for enhanced separation strategies in free-solution capillary electrophoresis setups, since we would expect the unfolding transition to modify the electrophoretic mobility dramatically. For a coupling constant $\Xi = 5$, which corresponds to a fully charged synthetic PE with monovalent counterions, the unfolding transition is less pronounced but is still significant experimentally since we expect the electrophoretic mobility to become monomer-number-independent for higher fields.

We also recorded the mobilities of monomers and condensed and uncondensed counterions. One of our main findings is that at small field strengths the condensed counterions are dragged along with the PE chain, while at elevated field strengths they start gliding along the chain. The mobility is controlled by electrostatic friction between the chain and condensed counterions and also by the asymmetry field due to the field-induced asymmetric counterion distribution. Since the gliding condensed counterions are contributing to the total conduction, the total conduction is larger than what one would expect if the condensed counterions were tightly bound to the PE chain. Conversely, an experimental estimate of the fraction of condensed counterions based on combined mobility and conduction measurements would give a lower number than expected on the basis of static theory alone. This is all true at field strengths of the order or above the unfolding/orientation threshold, which, however, is the case in most experimental situations.

The hydrodynamic interaction between moving particles has not been included on the present level of our theory but is presently under investigation.[19] According to our preliminary results, the unfolding transition is not shifted, at least for large coupling constants, since hydrodynamic effects are unimportant in the collapsed state. In the unfolded state, however, the mobilities are modified.

Our simulations have been performed without additional added co-ions, and the effective concentration of PE chains is controlled by our box size. Additional salt in the solution is able to inhibit globule formation at extremely large concentrations. At all experimentally relevant salt concentrations, the mechanism for the field-induced unfolding presented here is not modified, since the polarizability of the globule is always much higher than the polarizability of the salt solution.[19] The conduction properties in the oriented state (i.e., above the characteristic field strength $\tilde{E}^*$) will be influenced by the presence of salt due to a couple of mechanisms: first of all, the asymmetry field will be screened. Second, the binding of counterions on the PE chain will be looser because of screening, and therefore the electrostatic friction will be less pronounced. Most importantly, the total conduction will be more and more

dominated by the electrolyte solution, and the quite subtle effects discussed here would be hard to measure.

Acknowledgment. This work was financially supported by Deutsche Forschungsgemeinschaft (DFG, SFB 486) and the Fonds der Chemischen Industrie.

References and Notes

(1) Stevens, M.; Kremer, K. *J. Chem. Phys.* **1995**, *103*, 1669.
(2) Winkler, R. G.; Gold, M.; Reineker, P. *Phys. Rev. Lett.* **1998**, *80*, 3731.
(3) Khan, M. O.; Jönsson, B. *Biopolymers* **1999**, *49*, 121.
(4) Liu, S.; Muthukumar, M. *J. Chem. Phys.* **2002**, *116*, 9975.
(5) Olvera de la Cruz, M.; Belloni, L.; Delsanti, M.; Dalbiez, J. P.; Spalla, O.; Drifford, M. *J. Chem. Phys.* **1995**, *103*, 5781.
(6) Bloomfield, V. A. *Biopolymers* **1997**, *44*, 269.
(7) Raspaud, E.; Olvera de la Cruz, M.; Sikorav, J.-L.; Livolant, F. *Biophys. J.* **1998**, *74*, 381.
(8) Yamasaki, Y.; Teramoto, Y.; Yosjikawa, K. *Biophys. J.* **2001**, *80*, 2823.
(9) Stellwagen, N. C.; Gelfi, C.; Righetti, P. G. *Biopolymers* **1997**, *42*, 687.
(10) Viovy, J.-L. *Rev. Mod. Phys.* **2000**, *72*, 813.
(11) Elvingson, E. *Biophys. Chem.* **1992**, *43*, 9.
(12) Duke, T.; Viovy, J.-L. *Phys. Rev. E* **1994**, *49*, 2408.
(13) Semenov, A. N.; Joanny, J.-F. *Phys. Rev. E* **1997**, *55*, 789.
(14) Manning, G. S. *J. Phys. Chem.* **1981**, *85*, 1506.
(15) Long, D.; Viovy, J.-L.; Adjari, A. *Phys. Rev. Lett.* **1996**, *76*, 3858.
(16) Netz, R. R. *Phys. Rev. Lett.* **2003**, *90*, 128104.
(17) Olson, D. J.; Johnson, J. M.; Patel, P. D.; Shaqfeh, E. S. G.; Boxer, S. G.; Fuller, G. G. *Langmuir* **2001**, *17*, 7396.
(18) (a) Seyrek, E.; Dubin, P. L. Manuscript in preparation. (b) Huang, Q. R.; Dubin, P. L.; Moorefield, C. N.; Newkome, G. R. *J. Phys. Chem. B* **2000**, *104*, 898.
(19) Schlagberger, X.; Netz, R. R. Manuscript in preparation.
(20) Manning, G. S.; Mohanty, U. *Physica A* **1997**, *247*, 196.
(21) Manning, G. S. *Ber. Bunsen-Ges. Phys. Chem.* **1996**, *100*, 909.
(22) Solis, F. J.; Olvera de la Cruz, M. *J. Chem. Phys.* **2000**, *112*, 2030.
(23) Böttcher, C. J. F., Ed. *Theory of Electric Polarization*; Elsevier: Amsterdam, 1973.
(24) Kirkwood, J. G. *J. Polym. Sci.* **1954**, *12*, 1.
(25) Wien *Ann. Phys.* **1927**, *83*, 327.
(26) Katz, S.; Lebowitz, J. L.; Spohn, H. *Phys. Rev. B* **1983**, *28*, 1655.
(27) Krug, J. *Phys. Rev. Lett.* **1991**, *67*, 1882.
(28) Schmittmann, B.; Zia, R. K. P. *Phys. Rep.* **1998**, *301*, 45.
(29) Devore, D. I.; Manning, G. S. *J. Phys. Chem.* **1974**, *78*, 1242.
(30) Kim, J. M.; Ohtani, T.; Park, J. Y.; Chang, S. M.; Muramatsu, H. *Ultramicroscopy* **2002**, *91*, 139.
(31) Dewarrat, F.; Calame, M.; Schönenberger, C. *Single Mol.* **2002**, *3*, 189.
(32) Beyer, S.; Simmel, F. Manuscript in preparation.
(33) Kaes, J. Manuscript in preparation.
(34) Lachenmayer, K.; Oppermann, W. *J. Chem. Phys.* **2002**, *116*, 392.